



## Article

# The Characteristics and Seepage Stability Analysis of Toppling-Sliding Failure under Rainfall

Jing Luo , Xiangjun Pei \*, Ronghao Jiang, Tiantao Li, Hao Sun , Bo Jin and Qian Li

State Key Laboratory of Geohazard Prevention and Geoenvironment Protection,  
Chengdu University of Technology, Chengdu 610059, China

\* Correspondence: peixiangjun2012@cdut.cn; Tel.: +86-02884078689

**Abstract:** Toppling-sliding failure is a typical mode of deep-seated toppling failure. In this mode, massive collapsed rock masses form the main sliding body, which is sensitive to rainfall events and prone to instability under rainfall due to its unique slope structure. In the present study, based on the detailed investigation on the geology and deformation characteristics, we studied the deformation and failure mechanism of a large-scale deep-seated toppling in Nandongzi Village, Pingquan City, Hebei Province. We constructed an engineering geology model to describe the toppling-sliding failure under rainfall. In addition, based on the saturated–unsaturated seepage theory and using the SLOPE/W and SEEP/W modules in the GeoStudio software, we explored the seepage law and factors controlling the seepage failure of toppling-sliding under rainfall. From surface to interior, the slope can be divided into toppling-falling zone, strong toppling zone, slight toppling zone, and non-deformation zone. The geological structure consisting of an upper strong slab and an underlying weak rock layer, controls the early deformation, and the deformation and failure mode is compressing–bending–toppling. Due to the influence of excavation and rainfall, the sliding movements occur along planar rupture planes in the toppling-falling zone in the later stage, during which the failure mode switches to creeping–cracking. At present, the stability of the slope is highly sensitive to rainfall. When the rainfall intensity exceeds 220 mm/day (50 years return period storm), the factor of safety will fall below 1.05 and subsequently the sliding failure may be triggered. Because of the difference in permeability characteristics between the toppling-falling zone and the strong toppling zone, high pore-water pressure is developed at their boundary, leading to a drastic decrease in the factor of safety. Specifically, the more considerable difference in permeability, the lower the safety factor. Overall, this study is significant in scientific guiding for evaluating and preventing such slope failures.

**Keywords:** deep-seated toppling; toppling-sliding; rainfall intensity; slope stability; finite element method



**Citation:** Luo, J.; Pei, X.; Jiang, R.; Li, T.; Sun, H.; Jin, B.; Li, Q. The Characteristics and Seepage Stability Analysis of Toppling-Sliding Failure under Rainfall. *Sustainability* **2023**, *15*, 7736. <https://doi.org/10.3390/su15107736>

Academic Editor: Francesco Faccini

Received: 3 February 2023

Revised: 1 May 2023

Accepted: 4 May 2023

Published: 9 May 2023



**Copyright:** © 2023 by the authors. Licensee MDPI, Basel, Switzerland. This article is an open access article distributed under the terms and conditions of the Creative Commons Attribution (CC BY) license (<https://creativecommons.org/licenses/by/4.0/>).

## 1. Introduction

The occurrence of landslides is mainly influenced by geological conditions and external triggering factors, such as climate and human activities [1,2]. Landslides are mostly developed in mountainous areas and play a significant role in landscape evolution [3]. Notably, China's landslides are very active compared to those in other countries in the world due to China's complicated geological conditions [4]. In addition, landslides are one of the catastrophic geohazards that cause extensive economic, social, and environmental problems, posing a severe threat to local people directly [5]. Landslides have been ranked as the fourth deadly natural disaster commonly occurred after earthquakes, storms, and floods [6]. In recent years, an increase in the global mean temperature and the abrupt change in rainfall patterns have led to the occurrence of more shallow landslides [7].

Based on rock types and discontinuity patterns, Goodman and Bray [8] classified toppling into three modes: flexural toppling, block toppling, and block-flexure. Nichol et al. [9] suggested that “block toppling” will occur when a persistent cross joint is present, and can result in catastrophic failure. In contrast, “flexural toppling”, which is likely to be ductile,

will occur in the absence of a persistent cross joint. In the past decade, numerous large-scale construction projects in western China have been implemented, inevitably causing an increase in the number of rock slope instability characterized by toppling. Huang et al. [10] categorized toppling into three basic modes, i.e., deep-seated toppling, shallow toppling, and complex toppling, according to the deformation and failure process of toppling in light of the field data obtained from a large number of engineering projects. Huang et al. [11] systematically summarized the spatial distribution, formation conditions, and deformation characteristics of deep-seated toppling based on 49 cases in western China. Crosta [12] summarized the nomenclature problem, characteristic features, and differences in describing the phenomenon of deep-seated gravitational deformation based on more than 400 technical literatures. Crosta et al. [13] also constructed an inventory map of total 1033 deep-seated toppling cases in the entire European Alps.

Additionally, Huang et al. [10] divided the toppled slope body into toppling-falling zone, strong toppling zone, slight toppling zone, and non-deformation zone based on their different deformation/failure characteristics (i.e., tensile-shear fractures, tensile fractures, and relative reverse slip). The toppling-falling zone tends to evolve into sliding failures [11]. Glueer et al. [14] detailed an analysis of a deep-seated landslide, formed by rotation (toppling) of steep rock columns, where the shallow secondary rockslides within the deep-seated landslide show sliding movements along planar rupture planes and mixtures of both sliding and toppling. The toppling-sliding failure is mainly developed and observed in reservoir-rim slopes under the conditions of reservoir impoundment, reservoir drawdown, or heavy rainfall [15–18].

Rainfall is an important factor in triggering landslides [19–23]. It often leads to a rise in groundwater level or the development of the perched water zone, both of which may result in the reduction in soil matric suction (an increase in pore-water pressure). This, in turn, causes a decrease in the shear strength of soils, which is the direct reason for slope failure [24–26]. The toppling-falling zone has a high hydraulic conductivity because it is mainly composed of soil-rock mixture with loose cataclastic structure formed by the instability of the strong toppling zone. Therefore, the toppling-sliding failure mode may be susceptible to rainfall [27,28]. For example, the Nandongzi toppling was reactivated in 2017 due to the unloading effect produced by road excavation. To prevent the recurrence of failure, necessary countermeasures that include multi-stage excavation and drainage for stability improvement were completed in the Nandongzi slope at the beginning of 2019. However, new displacements were induced again by heavy rainfall in July 2019 and August 2020. The width, length, and volume of the Nandongzi toppling were estimated to be 200 m, 100 m, and 0.3 Mm<sup>3</sup>, respectively, posing a severe threat to local residents and transportation. Following are the objectives of this study: (1) illustrate and clarify the geology and deformation characteristics of the Nandongzi toppling; (2) construct an engineering geology model to describe the toppling-sliding failure mechanism under rainfall; (3) demonstrate the sensitivity of the safety factor to slope permeability and rainfall intensity. The above analysis and evaluation are essential for local disaster mitigation and socio-economic sustainability.

## 2. Geological Setting of the Study Area

The study area is located in the northeastern part of the North China Block. The area also belongs to the northern part of Hebei province, neighboring Peking to the west (Figure 1a). The geological map compiled by the China Geological Survey (1:200,000) shows Mesoproterozoic Changcheng Group (Chc) exposed in the Nandongzi toppling region; the group is dominated by quartz sandstone interbedded with thin-layered shale (Figure 1c). The average dipping angle/dip of bedding planes is 40°/345°. This region is located north of the Malanyu Anticline, the third-order structural unit of the Yanshan orogenic belt. The nearly NS-trending Fengjiadian-Laomaojia-Chagou fault, WNW-striking Laodujia fault, and Nanlaodong fault which is a reverse fault with a dipping angle/dip of 75–85°/275°, are all developed in the study area. In addition, the Huangzhangzi syncline

is exposed in the northern part of the Nandongzi toppling. The syncline belongs to the Changzhougou Group and has a strike of NNE–SSW ( $\sim 65^\circ$ ). The dipping angle/dip of the northwest and southeast flanks of the Huangzhangzi syncline is  $12^\circ/142^\circ$  and  $24^\circ/0^\circ$ , respectively. According to China's seismic parameter zoning map (GB 18306–2015), the seismic fortification intensity of the study area is VI.

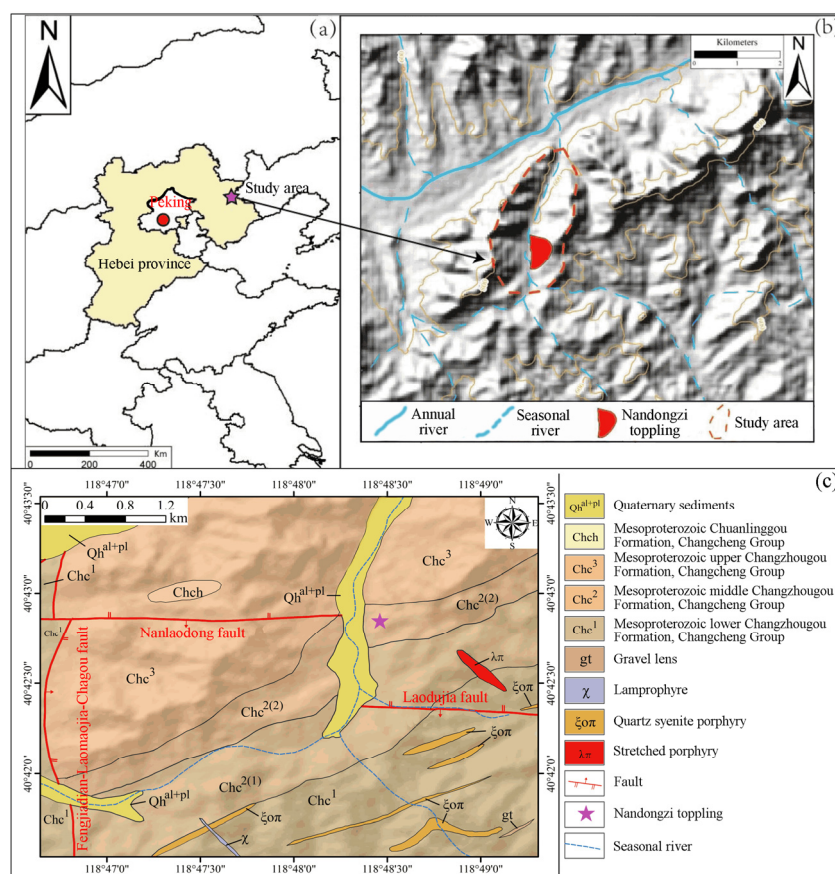


**Figure 1.** Geographical location and geological formation of the study area. (a) location of the study area; (b) location of the Nandongzi toppling; (c) geological formation of the study area.

The topography of the study area is generally high-steep in the northeast but low-flat in the southwest. A seasonal river, with an  $\sim 80$  m width valley, flows from north to south. However, the floodplains and terraces are not developed. The northeast ridge has the peak elevation of approximately 806 m asl, and the river valley has the lowest elevation of roughly 606 m asl, producing a maximum relief of 200 m. The mountains extend along the NE–SW direction. The elevation of the Nandongzi toppling ranges from 615 to 688 m asl and the corresponding slope is  $40^\circ$  (Figure 2).

The study area belongs to the warm temperate continental monsoon climate with four distinct seasons, i.e., windy springs, rainy summers, mild falls, and cold and dry winters. The average annual rainfall is 529.1 mm, with a maximum daily rainfall of 64.6 mm. The total rainfall in summer accounts for more than 80% of the annual rainfall. The annual average temperature is  $7.4^\circ\text{C}$ . The highest temperature ( $42.1^\circ\text{C}$ ) was recorded in July, and the lowest temperature ( $-31.4^\circ\text{C}$ ) was recorded in January. The main groundwater type is Quaternary pore phreatic water and bedrock fissure water. The groundwater level is highly dependent on the in situ rainfall, and thus the highest level is always observed from June to August. The groundwater mainly flows from south to north.

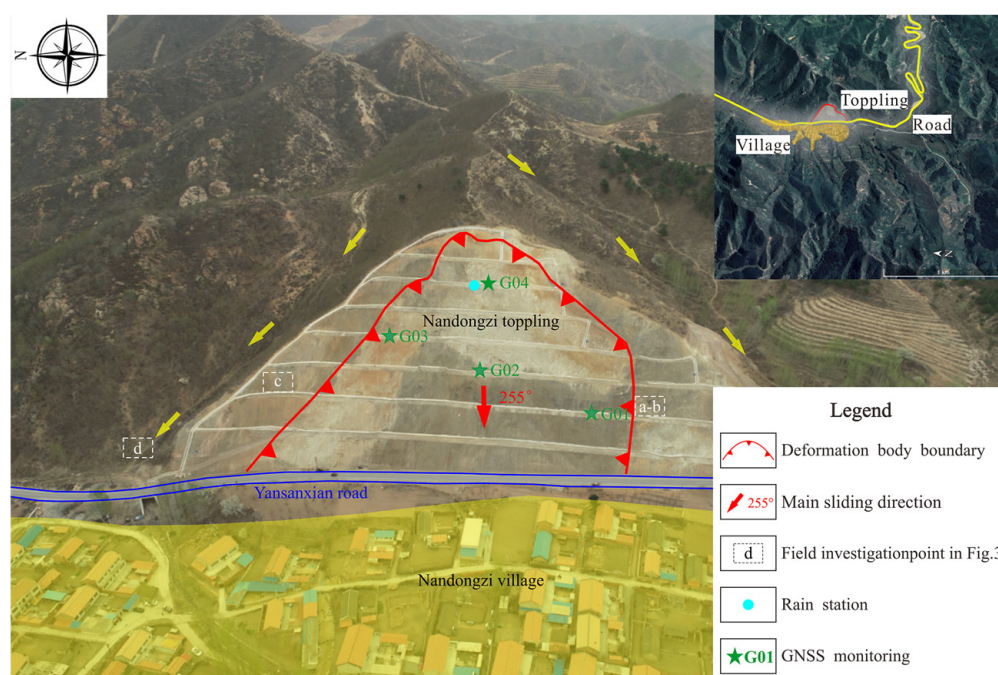


**Figure 2.** View of the Nandongzi toppling.

### 3. Characterization of the Nandongzi Toppling

Both the obvious bending folds and even the entirely fractured rock layers are highly developed in the Nandongzi toppling because it is located on the tectonically active south-east flank of the Huangzhangzi syncline and next to the Nanlaodong fault (Figure 3). Based on the varying rock quality designation (RQD) revealed by borehole drilling (the location of boreholes can be found in Figure 4), the degree of fragmentation and weathering rate is gradually getting higher from interior to the surface (Figure 5). The borehole drilling results, when combined with the detailed field investigation, revealed four distinct zones of the Nandongzi toppling: the toppling-falling zone, strong toppling zone, slight toppling zone, and non-deformation zone (Table 1). The toppling-falling zone ranges from 630 to 680 m asl and is mainly composed of quartz sandstone with loose cataclastic structures. The strong toppling zone ranges from 619 to 645 m asl, primarily consisting of siltstone and shale with apparent bending. The dipping angle of the rock layer in the middle of the toppling is nearly horizontal, while that in the north boundary of the toppling is  $70^\circ$  (Figure 6). Therefore, we suggest that the toppling direction is southwest. In addition, most of the borehole drilling results reveal a layer of wet and plastic silty clay with a thickness of about 20 cm at the bottom of the toppling-falling zone, indicative of the possible sliding surface (Figure 7).

**Table 1.** The characteristics of different zones of the Nandongzi toppling.

Index	Toppling-Falling Zone (A)	Strong Toppling Zone (B)	Slight Toppling Zone (C)	Non-Deformation Zone (D)
Fracture mechanism	Complete block detachment	Tensile-shear fracture	Tensile fracture	/
Deflection angle ( $^\circ$ )	/	15–35 $^\circ$	0–15 $^\circ$	0 $^\circ$
Unloading degree	/	Large	Medium	Small
Weathering degree	/	Intense	Moderate	Mild



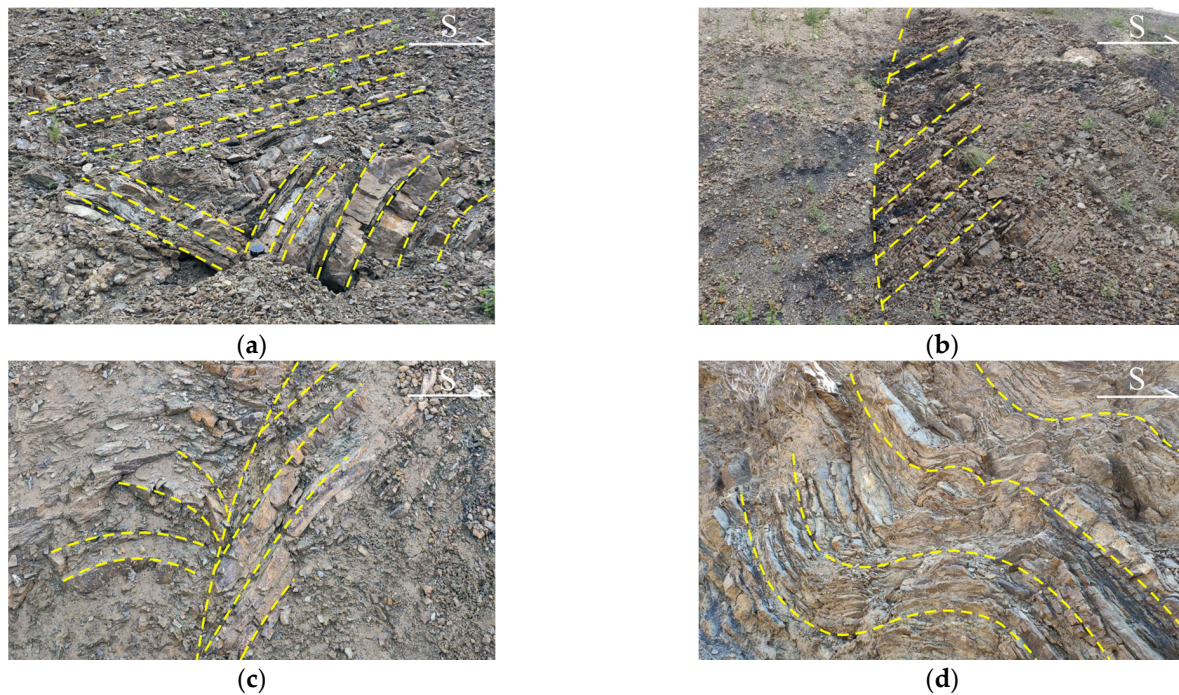


**Figure 3.** Typical bending and fracturing of the rock layers exposed on the slope surface. (a) complete fracturing; (b) different weathering degree; (c) obvious bending and fracturing; (d) bending folds.

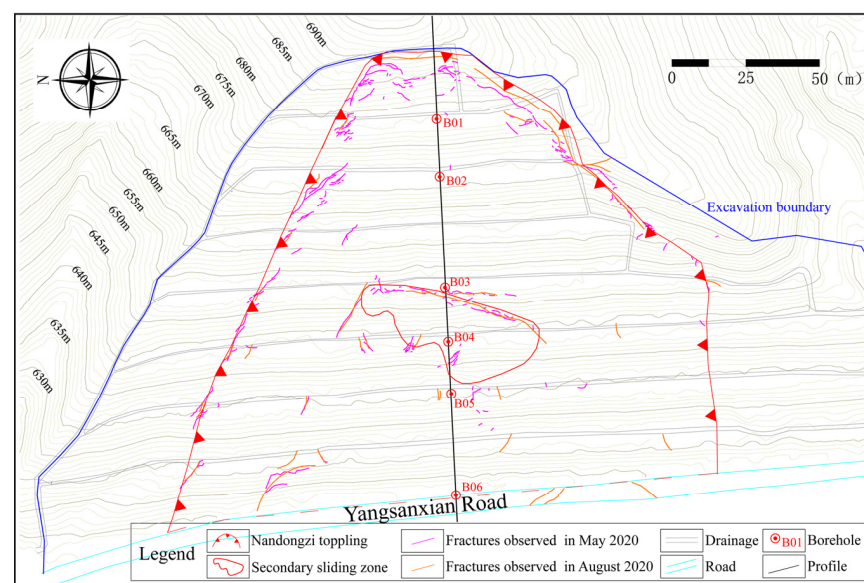


**Figure 4.** The distribution of multi-stage fractures.

The formation process of the Nandongzi toppling is recorded by satellite imagery. In June 2016, a road named Yansanxian was excavated at the foot of the Nandongzi slope. Due to the excavation-induced unloading effect, the Nandongzi slope toppled again in 2017. A tensile crack with a width of 5–10 cm was developed at the rear edge, with a range from 619 to 645 m asl. The necessary countermeasures consisting of multi-stage excavation and drainage to improve the stability of the Nandongzi slope were implemented in 2018 and completed in the beginning of 2019. However, in July 2019, heavy rainfall induced new displacements in the Nandongzi slope. Based on detailed field investigations carried out in May and August of 2020, there are apparent underground water outlets in the foot of the slope (from 1st step to 3rd step). In August 2020, the magnitude of displacement



was further enhanced, and the shear and tensile cracks expanded rapidly (Figure 8). The fractures can be divided into three types: (i) 2–3.5 m high headscarp with a length of about 30 m in the rear of the toppling; (ii) tensile fractures characterized by 1.3–1.5 m openings which have a total length of about 60 m developed in the middle of toppling; and (iii) side shear fractures which cut off drainage ditches (Figure 4).

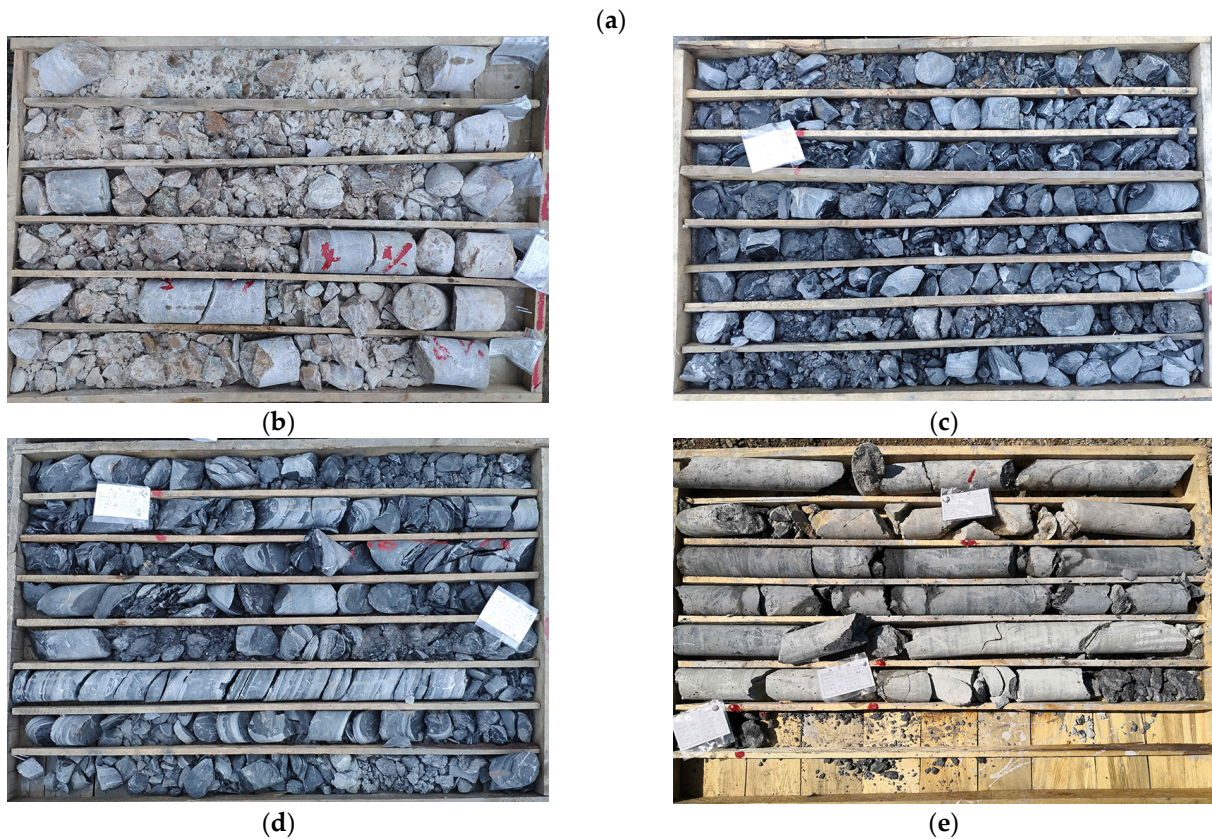
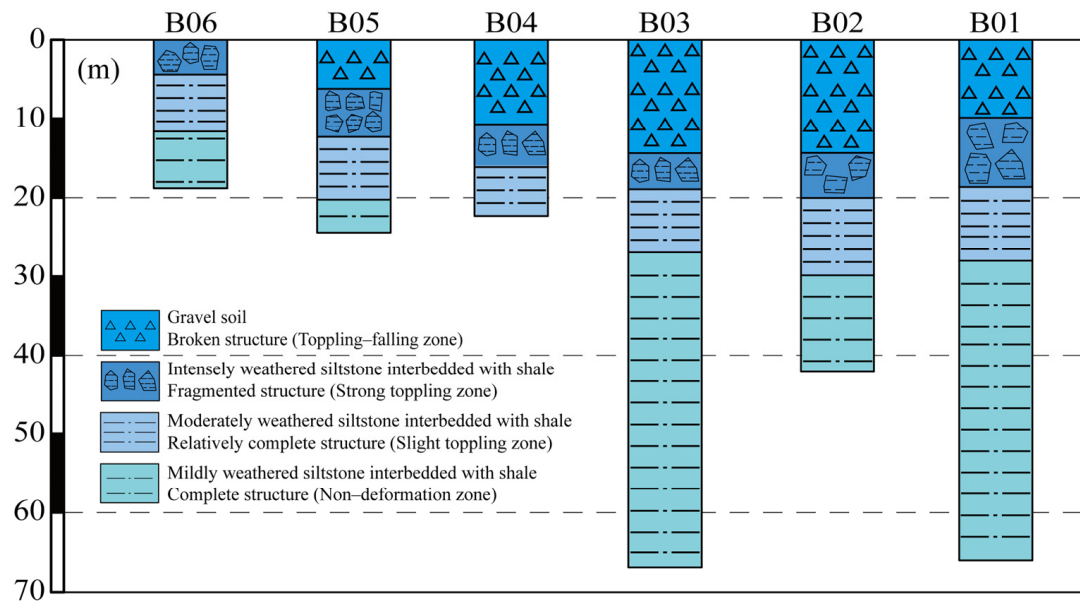


**Figure 5.** Lithological sections of six boreholes (a) (the locations of boreholes are shown in Figure 4), and typical photographs of drill core quality in toppling-falling zone (b), strong toppling zone (c), slight toppling zone (d), and non-deformation zone (e).





**Figure 6.** The deflection angle of the rock layer exposed on the slope surface, i.e., the evidence for the toppling.



**Figure 7.** Grayish white–white silty clay revealed by borehole drilling results at the bottom of the toppling-falling zone.



**Figure 8.** Deformation process revealed by remote sensing.

The formation process of the Nandongzi toppling basically includes two stages. Firstly, the progressive deformation of the Nandongzi toppling was controlled by geological structure, which consists of an upper strong thick-layer quartz sandstone and an underlying weak thin-layer siltstone interbedded with shale. The failure mode is compressing-bending-toppling [29]. Due to poor mechanical properties, the siltstone interbedded with shale is subject to bending under the compressive loading from the overlying strong quartz sandstone. Many release fractures in the quartz sandstone develop as a consequence of pre-failure progressive deformation in the underlying weak layer. Second, based on the high

degree of toppling, the toppling-falling zone slides along planar rupture planes dipping in the same direction as the slope under the influence of excavation and rainfall, during which the failure mode switches to creeping-cracking.

In addition, a high correlation was found between the displacement and rainfall data acquired at the Nandongzi toppling in 2020. The displacement increased sharply after the rainfall events in August, and remained in the nearly same level when there was no rainfall. Because the displacement results acquired by G02 and G04 are larger than those from others, we set their connection direction ( $275^\circ$ ) as the main sliding direction of the Nandongzi toppling. These data show that rainfall seepage plays the most dominant role in the deformation and failure of the Nandongzi toppling at this stage (Figure 9). As a result, it can be concluded that the toppling-falling zone will be saturated under rainfall due to its high permeability; however, the rock mass in the strong toppling zone is relatively intact and results in low permeability. Therefore, the pore-water pressure at the junction zone between the toppling-falling zone and strong toppling zone will sharply increase, thereby significantly reducing the slope stability under rainfall (Figure 10).

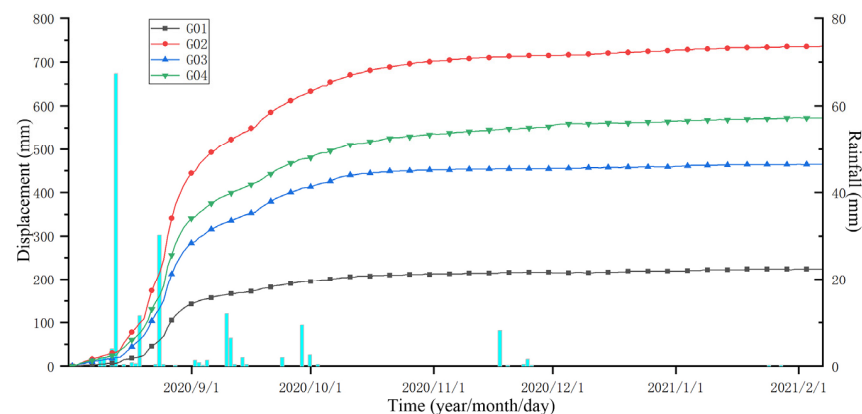


**Figure 9.** New displacement of the Nandongzi toppling and the in situ rainfall from July 2020 to February 2021.

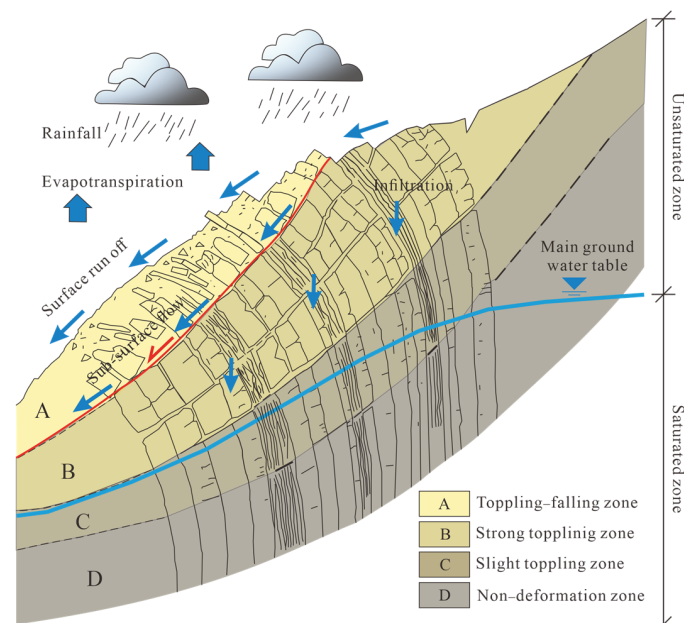


**Figure 10.** Engineering geology model displaying the toppling-sliding failure mechanism under rainfall (modified from Huang et al., [10]).



## 4. Seepage Stability Analysis Using Geo-Studio

### 4.1. Model Setup

The two-dimensional finite element program SEEP/W, which can model both saturated and unsaturated flows under steady-state and transient conditions, was adopted in the present study. According to the material composition, structural characteristics, and deformation characteristics, the numerical model of the Nandongzi toppling for seepage stability analysis was successfully constructed (Figure 11). The model comprises 1467 nodes and 1415 quadrilateral mesh elements (Figure 12). At the beginning of the transient seepage analysis, a hydrostatic condition was established based on the groundwater level revealed by borehole drilling. The water table assigned at 2 m below the ground surface would undoubtedly produce a realistically negative pore-water pressure (27 kPa) near the surface [30]. The left and right edges below the water table were assigned as head boundaries with pressure heads equal to 28 m and 90 m, respectively. In contrast, the left and right edges above the water table, as well as the bottom edge of the model were specified as no-flow boundaries. The rainfall-induced seepage was simulated by applying a unit flux ( $q$ ) of varying intensities on the exposed slope surface.

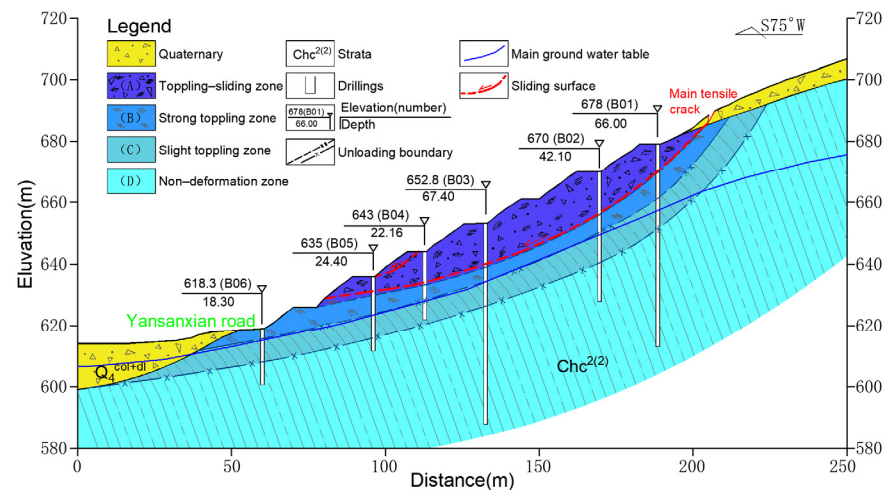


Figure 11. Geological profile of the Nandongzi toppling.

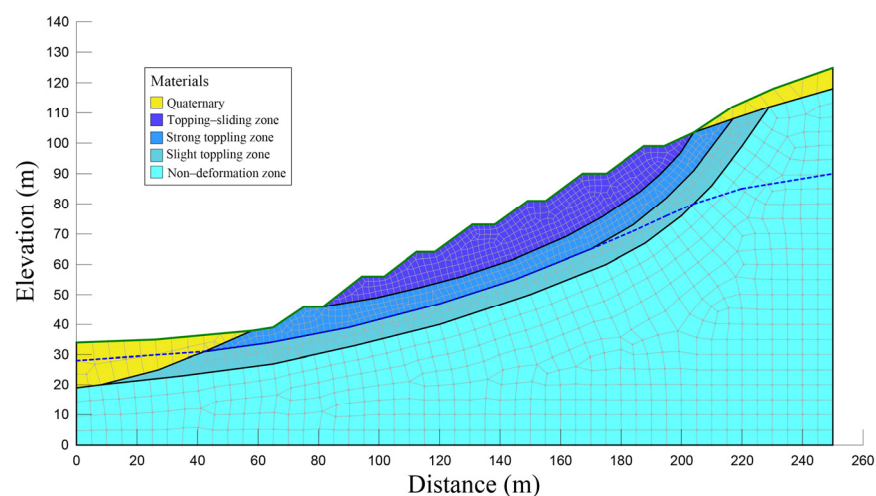


Figure 12. Numerical model of the Nandongzi toppling for seepage stability analysis.

SLOPE/W is a slope stability program that uses limit equilibrium analyses to determine the factor of safety. SIGMA/W is a stress and deformation analysis program that can solve linear elastic and nonlinear elastic-plastic deformation problems. In this study,

the pore-water pressure profile computed from the seepage analysis using SEEP/W was then integrated into slope stability analysis using SLOPE/W and deformation analysis using SIGMA/W. The horizontal displacement was fixed on the left and right edges of the model, while the vertical displacement was fixed on the bottom of the model. The factor of safety was obtained using the Bishop's simplified method that employs a modified Mohr–Coulomb failure criterion to realize the rainfall seepage-induced shear strength variation in the toppling-falling zone.

Because the influence of different rainfall patterns on slope stability are limited under similar rainfall intensity and duration [31], the steady and continuous rainfall condition was adopted. In addition, the 24 hour rainstorm contour map and Pearson-III distribution curve provided by the atlas of rainstorm statistical parameters in China (published by the Ministry of Water Resources and Nanjing Research Institute of Water Conservancy) were used to calculate the design rainstorms of four return periods, i.e., 5, 20, 50 and 100 years (Table 2), in order to analyze the effect of different rainfall intensities and permeabilities on the Nandongzi toppling. In fact, the amount of rainfall can vary substantially with the change of time and location. However, for the scope of the sensitivity analysis in this study, the exact magnitude of rainfall is not particularly important.

**Table 2.** Characteristic values of 24 h rainfall intensity corresponding to different return periods.

Return Period of 100 Years	Return Period of 50 Years	Return Period of 20 Years	Return Period of 5 Years
256 mm/day	220 mm/day	176 mm/day	108 mm/day

#### 4.2. The Properties of Rock and Soil Materials

In this study, we assumed that the transient water flow through unsaturated soils under rainfall infiltration obeys Darcy's law [32]. In unsaturated flow, the coefficient of permeability (hydraulic conductivity) is a function of water content or matric suction in unsaturated soils, which is conventionally assumed to be a constant in saturated soils [26].

SEEP/W includes a set of sampled volumetric water content (VWC) functions for soils with varying textures. The VWC functions adopted here correspond to gravel material with saturated water contents of 0.2, 0.25, and 0.3 for toppling-falling zone, strong toppling zone, and slight toppling zone, respectively (Figure 13). Based on the double-ring seepage tests operated in the toppling-falling zone and differential zonation characteristics of the toppled rock masses, the soil–water characteristic curves (SWCC) were then estimated using the Van Genuchten method [33], in which the saturated hydraulic conductivity ( $K_{sat}$ ) was specified as  $1 \times 10^{-4}$  m/s,  $1 \times 10^{-5}$  m/s, and  $1 \times 10^{-6}$  m/s for toppling-falling zone, strong toppling zone, and slight toppling zone, respectively (Figure 14). The Mohr–Coulomb model was applied in the toppling-falling zone, strong toppling zone, and slight toppling zone, while the “solid” model was utilized in the non-deformation zone. Based on the standard testing methods consisting of direct shear tests and unconfined compression tests operated in the laboratory, the strength and physical properties of rock and soil materials in different zones were determined through the trial-and-error “back analysis”. The trial-and-error “back analysis” was performed in terms of the monitored maximum rainfall (67.4 mm). We applied a flux value ( $Q$ ) of  $7.8 \times 10^{-7}$  m/s at the boundary for 24 h. The properties listed in Table 3 provided the modeled results (Figure 15) that best reproduced the real stability state and displacement from the field survey and monitoring (Figure 9). In detail, the overall factor of safety is 1.229 (Figure 15a), but the local factor of safety is 0.959 (Figure 15b), which almost coincides with the secondary sliding zone developed within the Nandongzi toppling (Figure 16); in addition, the maximum deformation displacement is approximately 0.85 m near the foot of slope (Figure 15c), which almost coincides with the monitored data from G02 (i.e., 0.73 m), and the deformation displacement is 0.43 m at the G04 monitoring site.

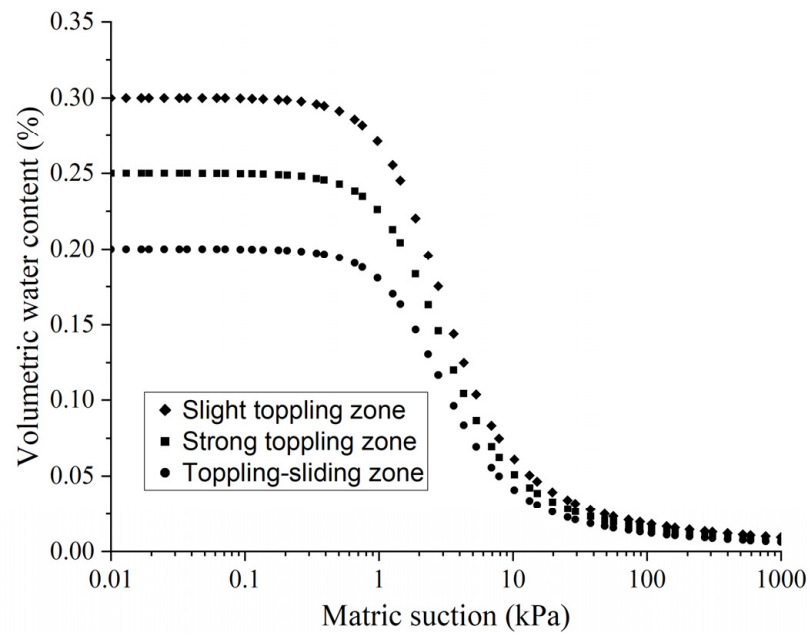


Figure 13. Permeability curve of the materials of three different zones.

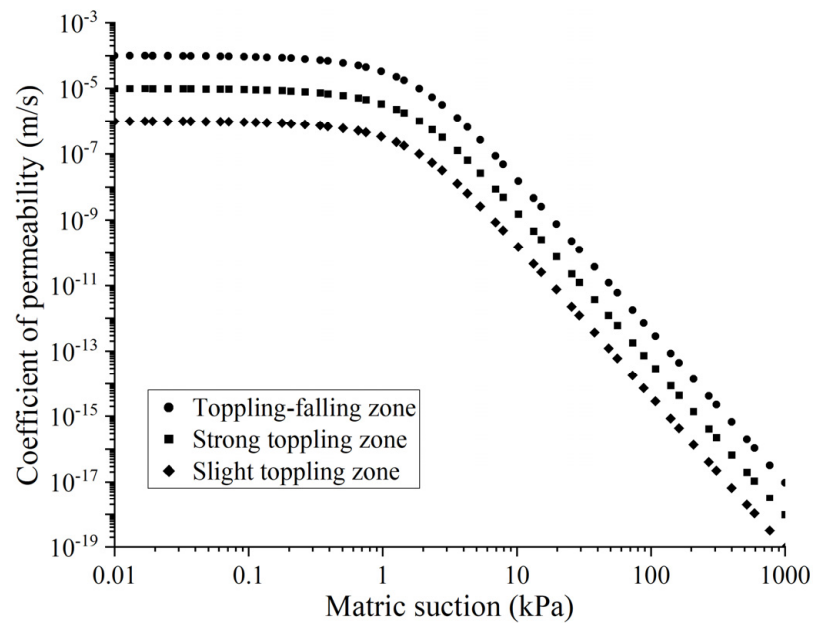
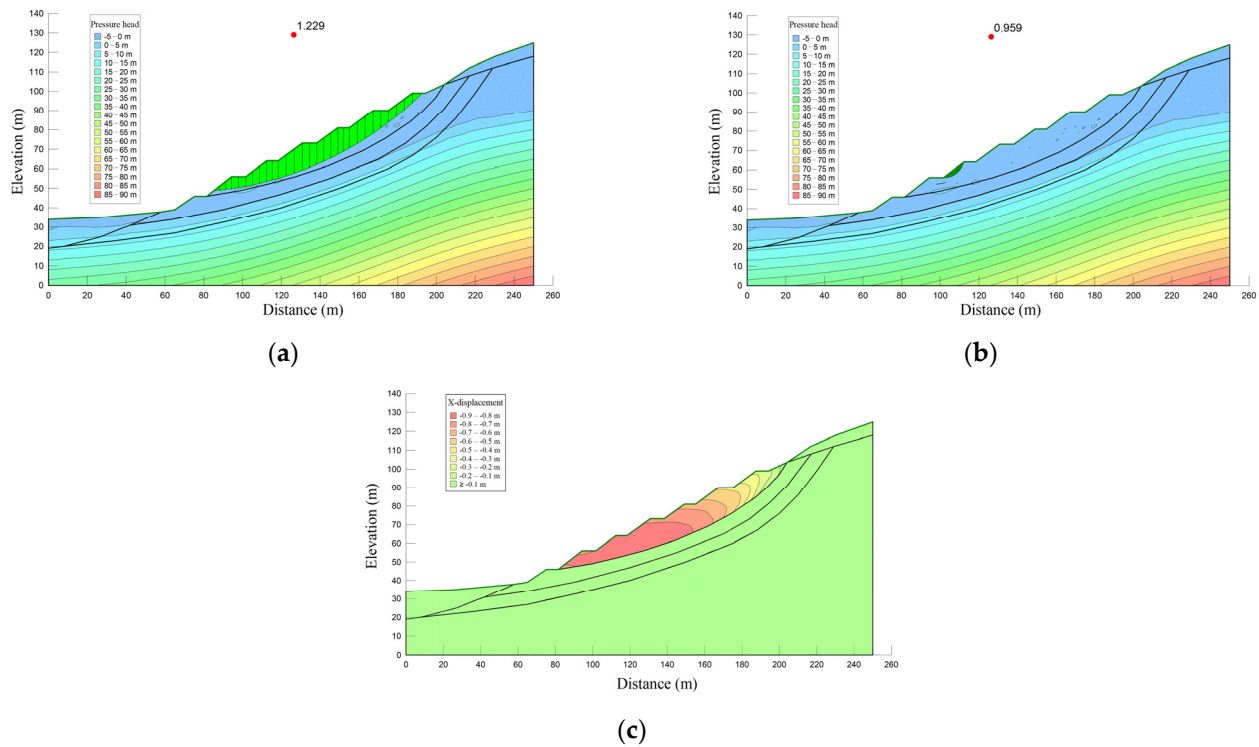


Figure 14. Soil-water characteristic curve (SWCC) of three different zones.

Table 3. Physical and mechanical parameters of rock and soil materials in different zones.

	Unit Weight/(kN/m <sup>3</sup> )	Cohesion/kPa	Angle of Friction/°	Saturated Volumetric Water Content/%
Toppling-falling zone	21.00	2.00	28.00	0.20
Strong toppling zone	22.00	5.00	32.00	0.25
Slight toppling zone	23.00	10.00	35.00	0.30
Non-deformation zone	24.00	20.00	40.00	0.30



**Figure 15.** Trial-and-error “back analysis” under different rainfall types (210 mm rainfall in 3 days). (a) the overall factor of safety; (b) the local factor of safety; (c) deformation displacement diagram of the slope.



**Figure 16.** A secondary sliding zone developed within the Nandongzi toppling showing the connection of the (a) steep tension fractures at the rear edge of the secondary sliding zone, (b) shear fissures along the bottom sliding surface and (c) lateral scarps.

Two stress state parameters, i.e.,  $(\sigma_n - \mu_a)$  and  $(\mu_a - \mu_w)$ , were initially introduced by Matyas and Radhakrishna [34] to describe the volumetric behavior of unsaturated soil.

On the basis of multi-phase continuum mechanics, Fredlund et al. [35] subsequently used the above two stress state parameters to analyze the stress of unsaturated soils. The pore-water pressure of the soil located above the water table is negative compared to the



atmospheric pressure [26]. To account for the effect of the negative pore-water pressure on the shear strength of soil and hence the factor of safety, Fredlund et al. [35] developed a modified Mohr-Coulomb failure criterion for unsaturated soils in terms of independent stress state variables and a constant value of  $\varphi^b$ , as follows:

$$\tau = c' + (\sigma_n - \mu_a) \tan \varphi' + (\mu_a - \mu_w) \tan \varphi^b$$

where,  $\tau$  denotes shear strength;  $c'$  is effective cohesion;  $\sigma_n$  is normal stress;  $\mu_a$  is pore air pressure;  $\varphi'$  is the effective angle of friction;  $\mu_w$  is pore-water pressure; and  $\varphi^b$  is the angle indicating the increase rate in shear strength concerning a change in matric suction.  $(\mu_a - \mu_w)$  is matric suction, which is crucial to the stability of unsaturated soil slope [36]. When this value is close to 0, the above formula represents shear strength for saturated soils.  $\varphi^b = 10^\circ$  was adopted in the limit equilibrium analyses.

#### 4.3. Numerical Modeling Results

Transient seepage analysis was performed under different return periods (5, 20, 50, and 100 years) using SEEP/W. The pore-water pressure profile computed from the seepage analysis was integrated into slope stability analysis using SLOPE/W, and the results are shown in Figure 17. Due to limited space, pore-water pressure distributions are not discussed in this study.

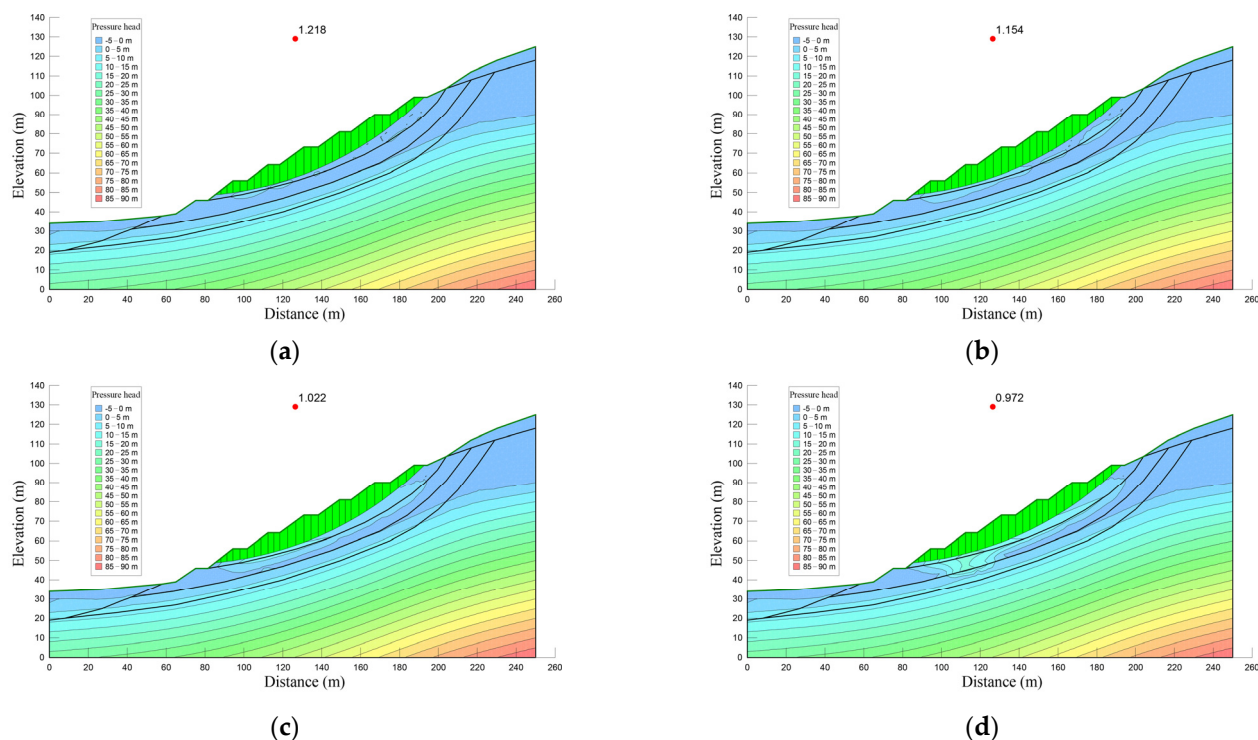


**Figure 17.** Slope stability under different rainfall intensities. (a) 5 years return period storm; (b) 20 years return period storm; (c) 50 years return period storm; (d) 100 years return period storm.

It appears that matric suction will not disappear and soils will hardly become saturated when the steady state rainfall is essentially less than the saturated hydraulic conductivity of the toppling-falling zone under five years return period storm (108 mm/day). The water flow direction is approximately perpendicular. Due to the soil's low moisture content and hydraulic conductivity, the rainwater seepage occur very slowly in the early stage of rainfall. The factor of safety changes slightly with the deepening of the wetting band until the wetting band reaches the strong toppling zone. Furthermore, the variation of hydraulic

conductivity forms a perched water zone, and high pore-water pressure is observed at the boundary between the toppling-falling zone and strong toppling zone. The amount and extent of pore-water pressure at the boundary between the toppling-falling zone and the strong toppling zone rise as rainfall intensity increases, thus leading to an increase in rainfall intensity and a reduction in the factor of safety.

For the 176 mm/day rainfall intensity (20 years return period storm), the factor of safety decreases to 1.154 which indicates a basically stable state. For the rainfall intensity of 220 mm/day (50 years return period storm), the pore-water pressure can be observed across the boundary between the toppling-falling zone and strong toppling zone, hence the factor of safety dropped to 1.022 (marginal stable state). For the rainfall intensity of 256 mm/day (100 years return period storm), seepage results in the rise of the main groundwater table, and hence the factor of safety further decreases to 0.972 (unstable state). Overall, rainfall intensity has a strong influence on the stability of the Nandongzi toppling, i.e., when the rainfall intensity exceeds 220 mm/day (50 years return period storm), the factor of safety will fall below 1.05 and the failure may be triggered.

In addition, different saturated coefficients of permeability of the strong toppling zone (i.e.,  $k_{sat1} = 1 \times 10^{-5}$ ,  $2 \times 10^{-5}$ ,  $5 \times 10^{-5}$ , and  $1 \times 10^{-4}$ ) were applied to study the effect of the ratio of  $k_{sat1}/k_{sat2}$  on the stability of the Nandongzi toppling, while saturated coefficients of permeability of the toppling-falling zone ( $k_{sat2} = 1 \times 10^{-4}$ , i.e., the ratio of  $k_{sat1}/k_{sat2} = 1:10$ ,  $1:5$ ,  $1:2$ , and  $1:1$ , respectively) and other conditions remain unchanged. It can be seen in Figure 18 that the factor of safety increases as the ratio of  $k_{sat1}/k_{sat2}$  increases, but the increase rates are affected by rainfall intensity. Notably, these rates are significantly greater in high rainfall intensity, suggesting that the ratio of  $k_{sat1}/k_{sat2}$  and rainfall intensity control the pore-water pressure, which the safety factor of the Nandongzi toppling is susceptible to, developed at the boundary between the toppling-falling zone and strong toppling zone.

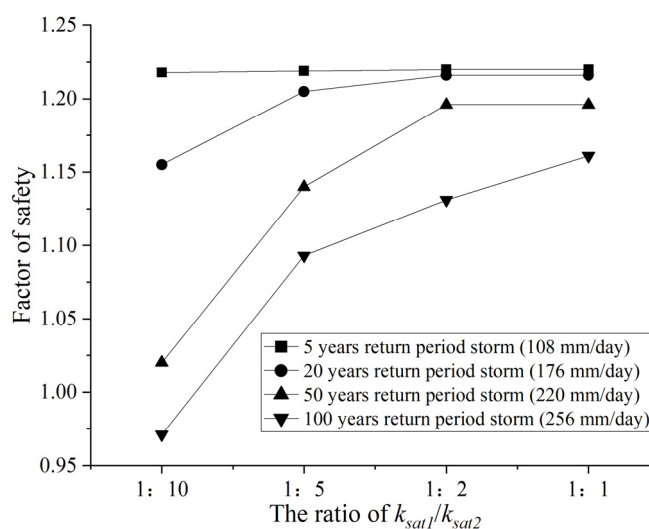


Figure 18. Slope stability under different rainfall intensities and the ratio of  $k_{sat1}/k_{sat2}$ .

## 5. Discussion

Based on the detailed investigation of the geology and deformation characteristics, the present study provides insight into the deformation and failure mechanism of a large-scale deep-seated toppling in Nandongzi Village, Pingquan City, Hebei Province. These analyses, when combined with the monitored data and numerical analysis, suggest that the stability of Nandongzi slope is highly sensitive to rainfall at present. Specifically, when the rainfall intensity exceeds 220 mm/day (50 years return period storm), the factor of safety will fall below 1.05 and slope failure may be triggered.

The strength and physical properties of rock and soil materials in different zones were determined through the standard laboratorial test and the trial-and-error “back analysis” according to the real stability state and deformation displacement. Such an integrated approach can improve the model accuracy in predicting the factor of safety of the Nandongzi toppling under different design rainstorms of return periods. Due to the fact that the toppling-falling zone is mainly composed of quartz sandstone with a loose cataclastic structure, the VWC functions adopted in the study correspond to gravel material in SEEP/W, with different saturated water contents for different zones. The SWCCs were then estimated using the Van Genuchten method with different saturated hydraulic conductivities. However, the hydraulic characteristics of block-gravel soil are distinctly different from those of gravel soil, and thus the Van Genuchten method may not be suitable to estimate the SWCCs in different zones of the Nandongzi toppling. In addition, the geographic uncertainty of rainfall data should be considered in the future. The relationship between the real displacement and rainfall data based on long-term multi-dimensional monitoring will help to reveal the formation mechanism, development process, and sensitive factors of such landslides. In summary, more investigations are required for more robust stability analysis of Nandongzi toppling, e.g., (1) the exploration adit, which is the best method to reveal inter structure of toppling and provide the opportunity for in situ test in other zones, should be operated; (2) the site-specific hydraulic properties in different zones should be directly established from the in situ or laboratorial test; etc.

## 6. Conclusions

In the present study, we constructed an engineering geology model to describe the toppling-sliding failure in Nandongzi Village under rainfall. Then, the seepage law and factors controlling seepage failure of toppling-sliding under rainfall were investigated by employing the SLOPE/W and SEEP/W modules in the GeoStudio software. Major conclusions from this study include the following:

1. From surface to interior, the Nandongzi slope can be divided into toppling-falling zone, strong toppling zone, slight toppling zone, and non-deformation zone.
2. The geological structure that consists of an upper strong slab and an underlying weak rock layer controls the early deformation. The deformation and failure mode is compressing-bending-toppling. In the later deformation stage, excavation and rainfall induce sliding movements along planar rupture planes in the toppling-falling zone of the slope, with the failure mode switching to creeping-cracking.
3. The ratio of  $k_{sat1}/k_{sat2}$  and rainfall intensity control the pore-water pressure developed in the boundary between the toppling-falling zone and strong toppling zone. The pore-water pressure further influences the safety factor of toppling-sliding slopes. The higher the ratio of  $k_{sat1}/k_{sat2}$ , the higher the safety factor.

It should be noted that the present study focused on investigating the effect of rainfall seepage on the stability of toppling-sliding slopes. Both evaporation and run-off which have significant impacts on rainfall seepage were not considered due to the lack of an effective method.

**Author Contributions:** All authors significantly contributed to the research. Conceptualization, J.L.; data curation, R.J., T.L. and H.S.; formal analysis, J.L. and R.J.; funding acquisition, J.L. and T.L.; methodology, J.L. and R.J.; resources, X.P.; software, J.L.; supervision, X.P. and J.L.; visualization, R.J., H.S. and Q.L.; Writing—Original draft, J.L., R.J. and B.J.; Writing—Review and editing, J.L. and X.P. All authors have read and agreed to the published version of the manuscript.

**Funding:** This research was funded by [National Natural Science Foundation of China] grant number [42107212 and 41907238] and [Natural Science Foundation of Sichuan Province] grant number [2022NSFSC1145].

**Institutional Review Board Statement:** Not applicable.

**Informed Consent Statement:** Not applicable.

**Data Availability Statement:** Data are available upon request from the corresponding author.

**Acknowledgments:** We gratefully acknowledge the Hebei Pingquan Natural Resources and Planning Bureau for their financial support to field investigation.

**Conflicts of Interest:** The authors declare no conflict of interest.

## References

- Görüm, T.; Fidan, S. Spatiotemporal variations of fatal landslides in Turkey. *Landslides* **2021**, *18*, 1691–1705. [\[CrossRef\]](#)
- Luo, J.; Pei, X.J.; Evans, S.G.; Huang, R.Q. Mechanics of the earthquake-induced Hongshiyan landslide in the 2014 Mw 6.2 Ludian earthquake, Yunnan, China. *Eng. Geol.* **2019**, *251*, 197–213. [\[CrossRef\]](#)
- Parker, R.N.; Densmore, A.L.; Rosser, N.J.; De Michele, M.; Li, Y.; Huang, R.; Whadcoat, S.; Petley, D.N. Mass wasting triggered by the 2008 Wenchuan earthquake is greater than orogenic growth. *Nat. Geosci.* **2011**, *4*, 449. [\[CrossRef\]](#)
- Tang, H.M. Advance and prospects of major landslides prediction and forecasting. *Bull. Geol. Sci. Tech.* **2022**, *41*, 1–13. (In Chinese)
- Alexander, D. Vulnerability to landslides. In *Landslide Hazard and Risk*; Glade, T., Anderson, M., Crozier, M.J., Eds.; Wiley: Hoboken, NJ, USA, 2005; pp. 175–198.
- Lacasse, S.; Nadim, F.; Kalsnes, B. Living with landslide risk. *Geotech. Eng. J. Seags Agssea* **2010**, *41*.
- Nadim, F.; Kalsnes, B.; Solheim, A. Plenary: Progress of living with landslide risk in Europe. In *Landslide Science for a Safer Geoenvironment*; Sassa, K., Canuti, P., Yin, Y., Eds.; Springer: Cham, Switzerland, 2014; pp. 3–20.
- Goodman, R.E.; Bray, J.W. Toppling of Rock Slopes. In Proceedings of the Specialty Conference on Rock Engineering for Foundations and Slopes, Boulder, CO, USA, 15–18 August 1976; Volume 2, pp. 201–234.
- Nichol, S.L.; Hungr, O.; Evans, S.G. Large-scale brittle and ductile toppling of rock slopes. *Can. Geotech. J.* **2002**, *39*, 773–788. [\[CrossRef\]](#)
- Huang, R.Q.; Li, Y.S.; Yan, M. The implication and evaluation of Toppling Failure in Engineering Geology Practice. *J. Eng. Geol.* **2017**, *25*, 1165–1181. (In Chinese)
- Huang, D.; Ma, H.; Huang, R.Q. Deep-seated toppling deformations of rock slopes in western China. *Landslides* **2022**, *19*, 809–827. [\[CrossRef\]](#)
- Crosta, G.B. Landslide, spreading, deep seated gravitational deformation: Analysis, examples, problems and proposals. *Geogr. Fis. Dinam. Quat.* **1996**, *19*, 297–313.
- Crosta, G.B.; Frattini, P.; Agliardi, F. Deep seated gravitational slope deformations in the European Alps. *Tectonophysics* **2013**, *605*, 13–33. [\[CrossRef\]](#)
- Glueer, F.; Loew, S.; Manconi, A.; Aaron, J. From toppling to sliding: Progressive evolution of the Moosfluh Landslide, Switzerland. *J. Geophys. Res. Earth Surf.* **2019**, *124*, 2899–2919. [\[CrossRef\]](#)
- Li, Y.; Yao, A.; Gong, Y. Deformation and Failure Mechanism of a Massive Ancient Anti-Dip River-Damming Landslide in the Upper Jinsha River. *Sustainability* **2022**, *14*, 13048. [\[CrossRef\]](#)
- Ning, Y.B.; Tang, H.M.; Zhang, G.C.; Smith, J.V.; Zhang, B.C.; Shen, P.W.; Chen, H.J. A complex rockslide developed from a deep-seated toppling failure in the upper Lancang River, Southwest China. *Eng. Geol.* **2021**, *293*, 106329. [\[CrossRef\]](#)
- Wang, F.; Tang, H.M. Mechanism and evolution of toppling in interbedded slopes at upstream of Yalong river. *J. Eng. Geol.* **2017**, *25*, 1501–1508. (In Chinese)
- Ren, G.M.; Xia, M.; Zeng, Q.; Jia, Y.; Lu, S.D.; Lu, D.L.; Liu, R.Q.; Zhao, H.Y.; Gou, F.M. Characteristics and formation mechanism of typical sliding-toppling landslides in Bailong River truck stream of Gansu, China. *J. Chengdu Univ. Tech. (Sci. Tech. Ed.)* **2015**, *42*, 18–25. (In Chinese)
- He, J.; Wang, S.; Liu, H.; Nguyen, V.; Han, W. The critical curve for shallow saturated zone in soil slope under rainfall and its prediction for landslide characteristics. *Bull. Eng. Geol. Environ.* **2021**, *80*, 1927–1945. [\[CrossRef\]](#)
- Kang, S.; Lee, S.R.; Cho, S.E. Slope Stability Analysis of unsaturated soil slopes based on the site-specific characteristics: A case study of Hwangryeong Mountain, Busan, Korea. *Sustainability* **2020**, *12*, 2839. [\[CrossRef\]](#)
- Li, S.; Qiu, C.; Huang, J.; Guo, X.; Hu, Y.; Mugahed, A.S.Q.; Tan, J. Stability Analysis of a High-Steep Dump Slope under Different Rainfall Conditions. *Sustainability* **2022**, *14*, 11148. [\[CrossRef\]](#)
- Lv, H.; Ling, C.; Hu, B.X.; Ran, J.; Zheng, Y.; Xu, Q.; Tong, J. Characterizing groundwater flow in a translational rock landslide of southwestern China. *Bull. Eng. Geol. Environ.* **2019**, *78*, 1989–2007. [\[CrossRef\]](#)
- Padilla, C.; Onda, Y.; Iida, T.; Takahashi, S.; Uchida, T. Characterization of the groundwater response to rainfall on a hillslope with fractured bedrock by creep deformation and its implication for the generation of deep-seated landslides on Mt. Wanitsuka, Kyushu Island. *Geomorphology* **2014**, *204*, 444–458. [\[CrossRef\]](#)
- Greco, R.; Marino, P.; Santonastaso, G.F.; Damiano, E. Interaction between perched epikarst aquifer and unsaturated soil cover in the initiation of shallow landslides in pyroclastic soils. *Water* **2018**, *10*, 948. [\[CrossRef\]](#)
- Marino, P.; Santonastaso, G.F.; Fan, X.; Greco, R. Prediction of shallow landslides in pyroclastic-covered slopes by coupled modeling of unsaturated and saturated groundwater flow. *Landslides* **2021**, *18*, 31–41. [\[CrossRef\]](#)
- Ng, C.W.W.; Shi, Q. A numerical investigation of the stability of unsaturated soil slopes subjected to transient seepage. *Comput. Geotech.* **1998**, *22*, 1–28. [\[CrossRef\]](#)



27. Zhang, L.L.; Fredlund, D.G.; Zhang, L.M.; Tang, W.H. Numerical study of soil conditions under which matric suction can be maintained. *Can. Geotech. J.* **2004**, *41*, 569–582. [[CrossRef](#)]
28. Zhang, Y.; Xu, W.Y.; Zou, L.F.; Sun, H.K. Analysis of seepage stability of large-scale landslide under rainfall condition. *Rock Soil Mech.* **2013**, *34*, 833–841. (In Chinese)
29. Alejano, L.R.; Gómez-Márquez, I.; Martínez-Alegría, R. Analysis of a complex toppling-circular slope failure. *Eng. Geol.* **2010**, *114*, 93–104. [[CrossRef](#)]
30. Lee, L.M.; Gofar, N.; Rahardjo, H. A simple model for preliminary evaluation of rainfall-induced slope instability. *Eng. Geol.* **2009**, *108*, 272–285. [[CrossRef](#)]
31. Zhang, D.Q.; Jiang, X.Y.; Zou, N.N.; Luo, B.J. Numerical analysis of colluvial landslide stability under the effect of rainfall infiltration: Taking Darong landslide of Guizhou Province for an example. *Sci. Tech. Eng.* **2019**, *19*, 338–344. (In Chinese)
32. Childs, E.C.; Collis-George, N. The permeability of porous material. *Proceedings of the Royal Society of London, A. Math. Phys. Sci.* **1950**, *201*, 392–405.
33. Van Genuchten, M.T. A closed-form equation for predicting the hydraulic conductivity of unsaturated soils. *Soil Sci. Soc. Am. J.* **1980**, *44*, 892–898. [[CrossRef](#)]
34. Matyas, E.L.; Radhakrishna, H.S. Volume change characteristics of partially saturated soils. *Geotechnique* **1968**, *18*, 432–448. [[CrossRef](#)]
35. Fredlund, D.G.; Morgenstern, N.R.; Widger, R.A. The shear strength of unsaturated soils. *Can. Geotech. J.* **1978**, *15*, 313–321. [[CrossRef](#)]
36. Fredlund, D.G.; Rahardjo, H. *Soil Mechanics for Unsaturated Soils*; John Wiley & Sons: Hoboken, NJ, USA, 1993.

**Disclaimer/Publisher’s Note:** The statements, opinions and data contained in all publications are solely those of the individual author(s) and contributor(s) and not of MDPI and/or the editor(s). MDPI and/or the editor(s) disclaim responsibility for any injury to people or property resulting from any ideas, methods, instructions or products referred to in the content.